Quaternary extension in the Rio Grande rift at elevated strain rates recorded in travertine deposits, central New Mexico

Jason W. Ricketts, Karl E. Karlstrom, Alexandra Priewisch, Laura J. Crossey, Victor J. Polyak, and Yemane Asmerom
DEPARTMENT OF EARTH AND PLANETARY SCIENCES, UNIVERSITY OF NEW MEXICO, MSC03-2040, 1 UNIVERSITY OF NEW MEXICO, ALBUQUERQUE, NEW MEXICO 87131-0001, USA

ABSTRACT

Calcite-filled extension veins and shear fractures are preserved in numerous travertine deposits along the western margin of the Albuquerque Basin of the Rio Grande rift. Calcite veins are banded and show geometries suggesting incremental cracking and calcite precipitation. U-series and ²³⁴U model ages from calcite infillings indicate that vein formation was active in the Quaternary, from ca. 2 Ma to ca. 250 ka. Vein orientations are systematic within each deposit and record a dominant extension direction that was horizontal and varied from E-W to NW-SE, consistent with both the regional finite extensional strain in the rift and with the global positioning system (GPS)-constrained deformation field. Three sites contain three orthogonal vein sets that crosscut one another nonsystematically, suggesting alternating times of: (1) regional E-W horizontal extension (dominant), (2) alternating N-S and E-W vertical veins that suggest vertical σ_1 and $\sigma_2 \approx \sigma_2$, and (3) horizontal veins that are interpreted to reflect times of highest pore fluid pressures and subequal principal stresses. One site contains conjugate normal faults that also record the dominant E-W extensional tectonic stress. Quaternary extensional strain rates calculated from vein opening for three locations range from $3.2 \pm 1.4 \times 10^{-16}$ s⁻¹ to $3.2 \times 10^{-15} \pm 2.7 \times 10^{-16}$ s⁻¹, which are up to ~40 times higher than the long-term (Oligocene–Holocene) finite strain rates calculated for different basins of the Rio Grande rift (8.5 x 10⁻¹⁷ to 4.5 x 10⁻¹⁶ s⁻¹), and up to ~100 times higher than modern strain rates measured by GPS data $(3.9 \times 10^{-17} \pm 6.3 \times 10^{-18} \text{ to } 4.4 \times 10^{-17} \pm 6.3 \times 10^{-18} \text{ s}^{-1})$. These high Quaternary rates are comparable to modern strain rates measured in the Basin and Range Province and East African Rift. Thus, this paper documents persistent E-W regional extension through the Quaternary in the Rio Grande rift that bridges geologic, paleoseismic, and GPS rates. Anomalously high strain rates in the Quaternary were facilitated by ascent of travertine-depositing CO2-rich waters along rift-bounding normal faults, leading to locally very high stain accumulations. These sites also provide examples of natural leakage of deeply sourced CO, interacting with regional tectonism, and they emphasize that rift maturation is a highly dynamic process, both spatially and temporally.

LITHOSPHERE; v. 6; no. 1; p. 3–16 | Published online 17 January 2014

doi: 10.1130/L278.1

INTRODUCTION

The N-S-trending Rio Grande rift, extending from Colorado to Mexico, provides an exceptional natural laboratory for understanding early stages and processes of continental rifting. Rifting began ca. 37–36 Ma (Kelley and Chamberlin, 2012), underwent maximum extensional activity in the Miocene based on ages of thickest Santa Fe Group rift fill (Chapin and Cather, 1994) and thermochronologic ages (Kelley et al., 1992), and is still active. Here, we address the processes that localize strain accumulation by documenting changes in strain rate through time. We also explore how temporal and spatial variations in extensional strain accumulation contribute to the heterogeneity of strain accumulation evident in continental rifts.

A persistent challenge for rift studies has been to bridge time scales in order to link rift evolution to rift processes. At the geologic time scale (tens of millions of years) required to accumulate the total extensional strain, restored cross sections can be drawn from geologic and seismic data, and these suggest extension magnitude varied from 30%–33% in the southern Albuquerque Basin (Russell and Snelson, 1994; Ricketts et al., 2011) to 17%–25% in the northern Albuquerque Basin (Russell and Snelson, 1994; Roy et al., 1999) to 8%–12% in the San Luis Basin (Kluth and Schafenaar, 1994). At the thousand(s) of year time scale, paleoseismic studies are sometimes available by trenching across Quaternary faults to constrain slip history and recurrence intervals. For example, in the Rio Grande rift,

recurrence intervals of \sim 20–40 k.y. and slip rates of \sim 0.027–1 mm/yr have been estimated for the late Quaternary (McCalpin, 2005; McCalpin et al., 2011; Olig et al., 2011). At the decade scale, data from continuous recording of global positioning system (GPS) have been successful at modeling the present-day strain directions and rates, which show the rift is currently extending at rates of \sim 0.12 mm/yr (Berglund et al., 2012).

This paper examines several questions regarding the history and processes of strain accumulation in the Rio Grande rift: (1) Is the Rio Grande rift still extending in the Quaternary? (2) If so, were the paleostrain and paleostress directions consistent with the generally E-W extension inferred at longer and shorter time-scale studies? (3) What were Quaternary strain rates? (4) What roles do fluids play in the extensional process, and what are their sources (endogenic vs. epigenic or meteoric fluids)? Here, we show that rift maturation is a highly dynamic process, both spatially and temporally. Further, the rifting process can be highly influenced by fluid flux through fault systems, which can create elevated pore fluid pressures, modify the local stress field by reducing the effective normal stress, and hence facilitate fault slip and strain accumulation rates (e.g., Hubbert and Rubey, 1959; Malagnini et al., 2012).

GEOLOGIC SETTING

The Rio Grande rift is a N-S-trending continental rift that separates the Colorado Plateau to the west from the Great Plains physiographic province to the east. The rift is a narrow structure tens of kilometers wide and is composed of individual half grabens that alternate polarity from north to south. In northern New Mexico, the rift crosses the Jemez Lineament and continues south, where it widens south of Socorro, New Mexico, into a broad zone where strain is distributed among multiple adjacent graben and half-graben systems of the Basin and Range Province (Fig. 1; e.g., Seager et al., 1984). This transition between the narrow Rio Grande rift and the highly extended Basin and Range Province is also the location of the Socorro magma body, a thin midcrustal magma sheet, located

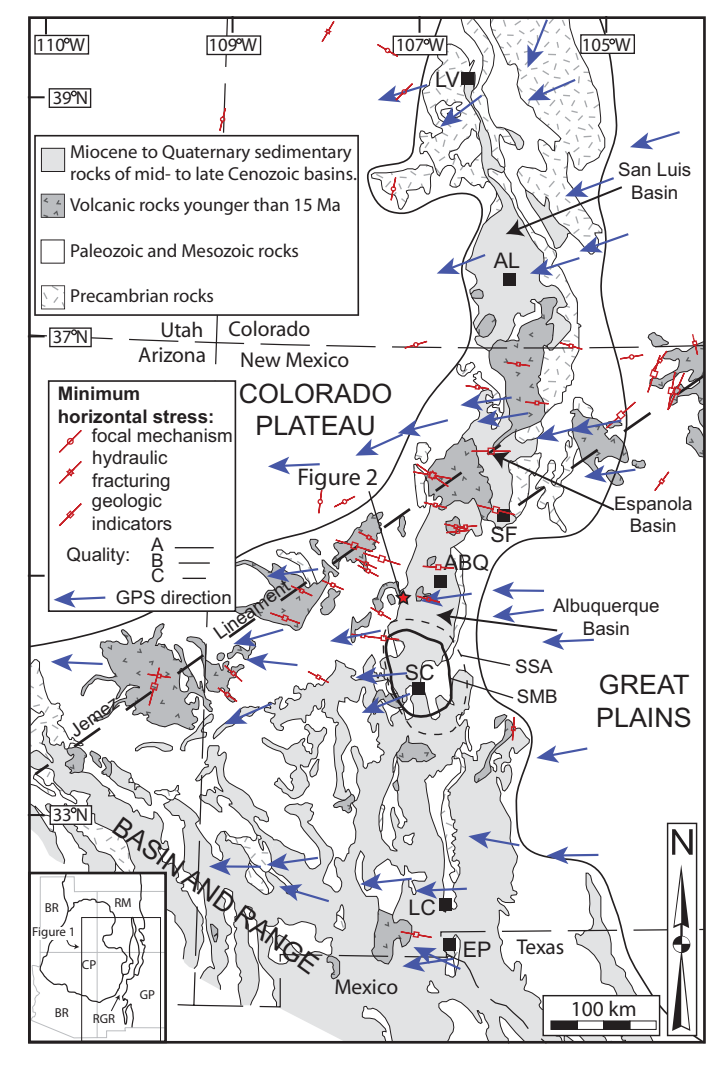


Figure 1. State of stress and strain in the Rio Grande rift region shown on a regional geologic map. Study area is shown by star on the western margin of Albuquerque Basin. Precambrian rocks (hachured pattern) and Miocene to Quaternary sedimentary rocks (light gray) define the N-S-trending Rio Grande rift. In red are modern and young stress orientations from the World Stress Map, which show the minimum horizontal stress direction (extensional direction of strain). Geologic indicators used in the World Stress Map are generally Quaternary in age (Heidbach et al., 2008). Blue arrows are extension directions measured from global positioning system (GPS; Berglund et al., 2012). Map is modified from Baldridge et al. (1984). LV—Leadville; AL—Alamosa; SF—Santa Fe; ABQ—Albuquerque; SC—Socorro; LC—Las Cruces; EP—El Paso; SMB—Socorro magma body; SSA—Socorro seismic anomaly. Inset shows the Rio Grande rift (RGR) in relation to the Basin and Range Province (BR), Colorado Plateau, (CP), Rocky Mountains (RM), and Great Plains (GP).

19 km deep, having horizontal dimensions of 50–70 km (Sanford et al., 1973; Reinhart and Sanford, 1981; Balch et al., 1997). Associated with the Socorro magma body is the Socorro seismic anomaly. The Socorro seismic anomaly covers ~2% of the state of New Mexico, yet produces ~45% of its seismic events above magnitude 2.5 (Balch et al., 1997). In addition, vertical uplift directly over the Socorro magma body has been persistent at ~2–5 mm/yr for over a century, with uplift diminishing to zero radially outward (Larsen and Reilinger, 1983; Larsen et al., 1986; Fialko and Simons, 2001). These data suggest that the region is still magmatically and seismically active.

Our study site is located along the western margin of the Albuquerque Basin of the Rio Grande rift in central New Mexico just north of the Socorro magma body and seismic anomaly (Figs. 1 and 2). This is an important region for neotectonic studies because the rift flank here is characterized by a relatively narrow (<1 km) zone of several well-exposed faults that are bounded to the west by the Colorado Plateau and to the east by Santa Fe Group basin fill sediments; Pliocene basalts and Quaternary travertines straddle the rift flank here and provide age control on faulting history. Within this zone, E-W compression during the Laramide orogeny produced a set of N-S-trending folds and reverse faults, the most prominent of which is the Comanche fault, a west-dipping high-angle structure separating the Permian Madera Group from Pennsylvanian Abo and Yeso Formations (Fig. 2; Callender and Zilinski, 1976). Most of these early-formed reverse faults, including the Comanche fault, were subsequently reactivated or overprinted during extensional deformation related to Neogene development of the Rio Grande rift (Lewis and Baldridge, 1994). Today, the main rift-bounding normal fault in the study area is the ~55°E-dipping Santa Fe fault, which separates Santa Fe Group synrift deposits to the east from Paleozoic and Mesozoic strata of the Colorado Plateau to the west (Fig. 2; May and Russell, 1994). In some areas, the Santa Fe fault offsets Pliocene-early Pleistocene Santa Fe Group rift-fill deposits (Lozinsky and Tedford, 1991). In contrast, a 3.7 ± 0.4 Ma basalt flow (Bachman and Mehnert, 1978) overlies fault strands of the Comanche fault zone and is not offset by these structures, indicating that Quaternary movement was concentrated along the Santa Fe fault zone (Fig. 2).

Travertine mounds and active springs precipitating travertine are preserved along much of the western margin of the Albuquerque Basin. They straddle the rift-bounding faults and blanket much of the older strata and structure, especially in the southern parts of the study area. They are fanshaped deposits in map view with uphill apex (likely now-extinct spring vents) located along the Comanche fault, but without any observable offset related to growth of the Santa Fe or Comanche fault systems. The close association of these travertine deposits with rift-related structures, and the existence of nearby active travertine-depositing springs within arroyos along multiple fault strands suggest that these platforms were deposited from spring waters emanating from the Comanche-Santa Fe fault system (Fig. 2; Callender and Zilinski, 1976). Springs that formed these deposits are no longer flowing, and fan apexes are situated above the modern valley floor (Qa to the west of travertine deposits in Fig. 2) as a result of recent and ongoing denudation of the Albuquerque Basin, which accelerated between 1.2 and 0.7 Ma and was likely facilitated by climatic changes related to the onset of glaciations in the headwaters of the Rio Grande (Connell, 2004). Additional topographically high erosion surfaces present within the study area are composed of probable Quaternary-aged sandstone and conglomerate beds containing locally derived clasts that are cemented with travertine, and as a result, also exist as terraces preserved above the modern valley floor.

The large-volume travertine deposits of this study are presently inactive (dry), but smaller-volume, actively precipitating travertine deposits are found nearby at low elevation along active springs within Arroyo

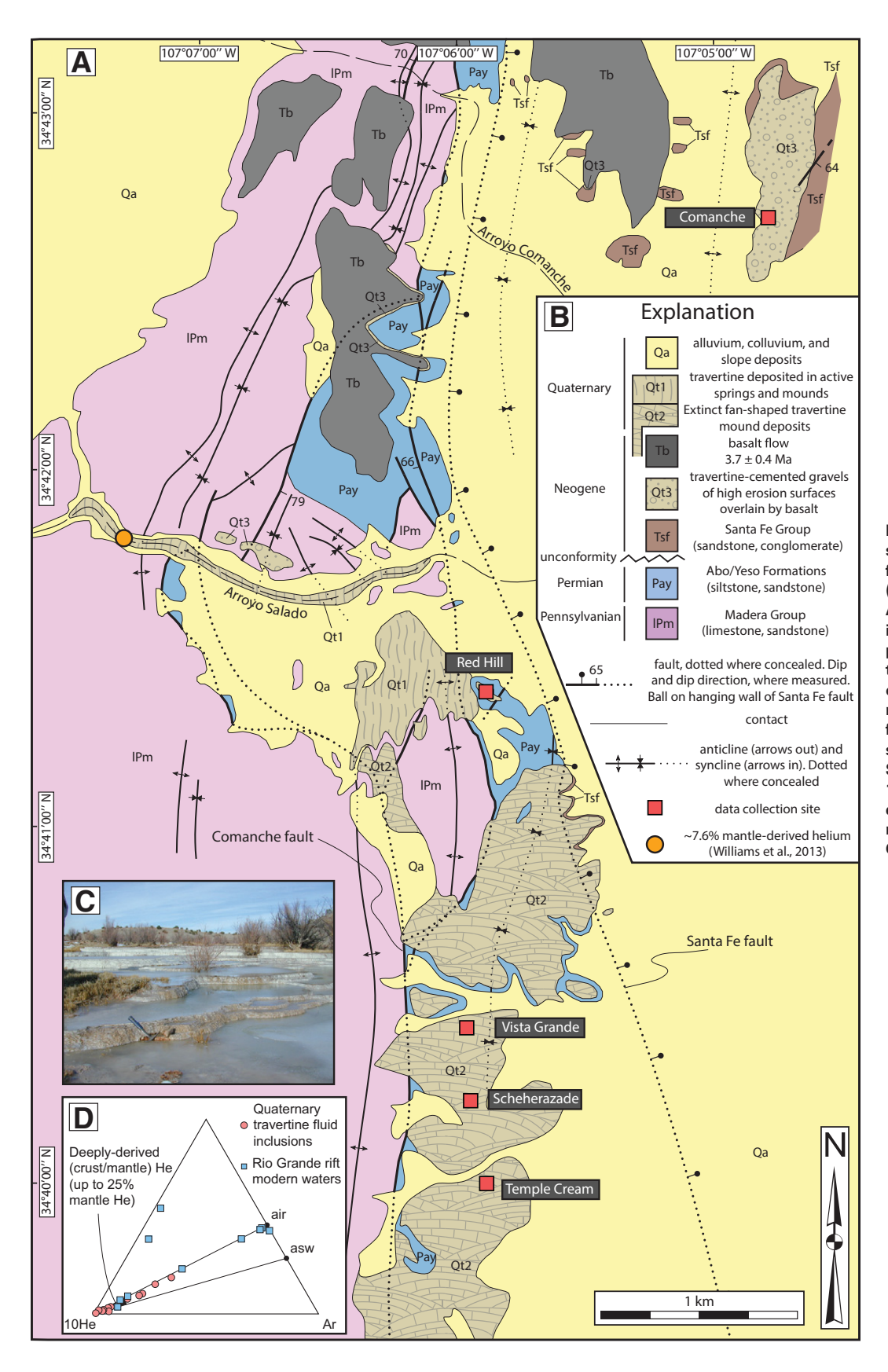


Figure 2. (A) Geologic map of study area. Basalt K-Ar age is from Bachman and Mehnert (1978). (B) Map explanation. (C) Actively precipitating travertine in Arroyo Salado. (D) He-Ar-N₂ plot (after Giggenbach, 1992) for travertine-spring gases from various locations in the Rio Grande rift (from Newell et al., 2005) and from gas analysis of fluid inclusions in vein calcite at quarry site Scheherazade (from Gundimeda, 1995). Fields for crust/mantlederived gases, air, and air-saturated groundwater (asw) are from Giggenbach (1992).

Salado and Arroyo Comanche to the north (Fig. 2). These springs are also aligned on the same faults and provide an analogy for the types of springs that deposit travertine. They have similar dams, coatings on vegetation, drapes, and travertine facies to those preserved in the older mound and platform deposits. The main difference in morphology between these and the extinct travertine fans is that they occur where faults intersect arroyo bottoms rather than closely spaced and strung out along a short fault segment. This likely reflects the ongoing stream incision into the rift flank in the last 1–2 m.y. and relatively dry paleohydrology conditions (and hence low head) in the Holocene.

Recent work on similar travertine deposits and modern travertinedepositing carbonic springs in the southwest United States indicates that source fluids are a mixture of both meteoric (epigenic) and deeply sourced (endogenic) fluids (Crossey et al., 2006, 2009; Williams et al., 2013), and that the endogenic fluids are conveyed to the surface along basement-penetrating faults (Crossey et al., 2006). Endogenic fluids that deposit travertine are typically slightly warm (~22-31 °C), are rich in dissolved CO₂ (pCO₂ values as great as 10^{0.1}), and contain mantle ³He as part of the trace gases (Crossey et al., 2006). In central New Mexico, the high CO₂ and accompanying trace gases in endogenic waters in active springs are interpreted to be a result of mantle degassing, and are brought to the near-surface through shallow microseismic events associated with the Socorro magma body and Socorro seismic anomaly (Newell et al., 2005; Williams et al., 2013). Within the study area, ³He values of Arroyo Salado waters indicate ~7.6% mantle-derived helium (Williams et al., 2013), and gas abundances from fluid inclusions in travertine at Scheherazade plot within the field of crust-mantle input (Gundimeda, 1995), and overlap with gas abundances measured in modern travertine-depositing springs with a known endogenic component (Fig. 2; Newell et al., 2005).

STUDY SITES

Some of the largest inactive travertine mounds that were previously discussed are currently being quarried by New Mexico Travertine, Inc., providing a spectacular display of the internal geometries at several locations (Fig. 3). Three of these quarry sites (Temple Cream, Scheherazade, and Vista Grande), as well as two additional travertine-cemented terraces north of the quarry sites (Red Hill and Comanche), were chosen as study sites. All of these study sites are currently inactive in terms of travertine deposition. The location of these travertine deposits along rift-flanking faults, and their datable record of progressive vein development offer an exceptional field laboratory to test models for fault connections among deeply sourced CO, magmatic fluids, fault conduits, carbonic springs, and large-volume travertine deposition (Crossey et al., 2009, 2011; Williams et al., 2013; Priewisch et al., 2012). They also offer an opportunity to estimate accumulated strains associated with Quaternary extension in the Rio Grande rift at this location.

At three quarry sites, Temple Cream, Scheherazade, and Vista Grande, abundant veins of different orientations cut the horizontal sedimentary layering of the travertine platforms. The majority of these veins range from ~1 mm to 10–20 cm in width perpendicular to the vein wall, and they are almost completely filled with sparry calcite, with little to no detrital material. Bedding layers along either side of the veins are offset perpendicular to the walls of the veins, with little shear offset, suggesting that most veins are purely extensional (e.g., Fossen, 2010). Multiple generations of crosscutting extensional veins are preserved at these three sites (Figs. 3E and 3F), each with a significant accumulation of vein fill and well-developed calcite banding that records multiple deformation events. In thin section, extensional veins from the quarry sites display both syntaxial and antitaxial growth (Ramsay and Huber, 1983). Syntaxial veins display a well-developed median line, and elongate calcite fibers grow from the vein wall inward. In contrast, antitaxial vein growth is suggested by radiating calcite fibers that grow from the center of the vein toward the vein wall (Fig. 4). Both suggest incremental deformation and subsequent sealing of cracks by precipitation.

An important morphologically and lithologically different site is Red Hill, the flanks of which are composed of reddish-purple-brown fine sandstones and siltstones of the Permian Yeso Formation. These Permian rocks are capped by ~2–3-m-thick travertine deposits that overlie older/elevated terrace gravels from the nearby arroyo that stand ~20 m above Arroyo Salado (Figs. 2 and 3). Abundant calcite-filled extensional veins ~1 mm to 10 cm in thickness cut both the Yeso Formation and the overlying travertine deposit, indicating their Quaternary age. Some small-offset (<1 m shear displacement) faults are observed within the Yeso Formation, but they do not offset the overlying travertine. These faults form conjugate pairs, as evidenced by oppositely dipping faults that crosscut one another. They display normal-sense displacement and preserve well-defined slickenside surfaces (Fig. 3D). In addition to <1 m of shear offset, many of the faults observed also display a component of extension perpendicular to the walls of the fracture, as evidenced by ~1-4 cm of calcite that has precipitated along the slip surface. The final location, Comanche platform, is a resistant cap consisting of well-cemented sandstone, pebble to cobble conglomerate containing clasts of local Paleozoic rocks, and travertine. Travertine deposits at this location are mostly in the form of infillings that cement the siliciclastic material, but there are also abundant extensional veins, which are orthogonal to sedimentary bedding as defined by sandy beds. Veins range from ~2 cm to 20 cm in thickness and are filled predominantly with calcite, and little to no detrital material.

We used the travertine deposits at these five locations, coupled with their associations with the Comanche and Santa Fe fault systems, to explore the significance of fractures and veins in the travertine. Given that the 3.7 \pm 0.4 Ma basalts in the study area locally overlie fault strands of the Comanche fault zone (Fig. 2; Callender and Zilinski, 1976), and that the timing and amount of Quaternary slip are only poorly documented on the Santa Fe fault, the fractures and veins in travertine provide a record of previously undocumented and quantifiable young tectonism in the zone between the Santa Fe and Comanche faults along the western margin of the Albuquerque Basin of the Rio Grande rift.

METHODS

Systematic extensional vein orientation measurements and observations were made at five locations. Sites were chosen (1) to cover a range of different locations along curvilinear faults to test possible stress rotations due to fault orientation, (2) to cover a range of slope aspects to test possible stress contributions from topographically driven gravitational stresses, and (3) to include sites dominated by extensional veins as well as conjugate faults to utilize different methods for estimating paleostress.

At Red Hill, slip magnitudes are generally less than ~1 m, so the movement direction was constrained by matching offset bedding layers. Poles to extensional veins from Temple Cream, Scheherazade, Vista Grande, Red Hill, and Comanche were plotted on lower-hemisphere, equal-area stereographic projections using Stereonet software. Similarly, faults at Red Hill were plotted as planes using FaultKin software (Marrett and Allmendinger, 1990; Allmendinger et al., 2012). Statistical analysis of normal faults and extensional veins was computed by means of a Bingham axial distribution (Mardia, 1972). The eigenvalues are a measure of the relative concentrations of measured veins and faults and indicate significant extensional directions. Thus, the eigenvalues can be used to quantify the extension directions that are most significant given the population

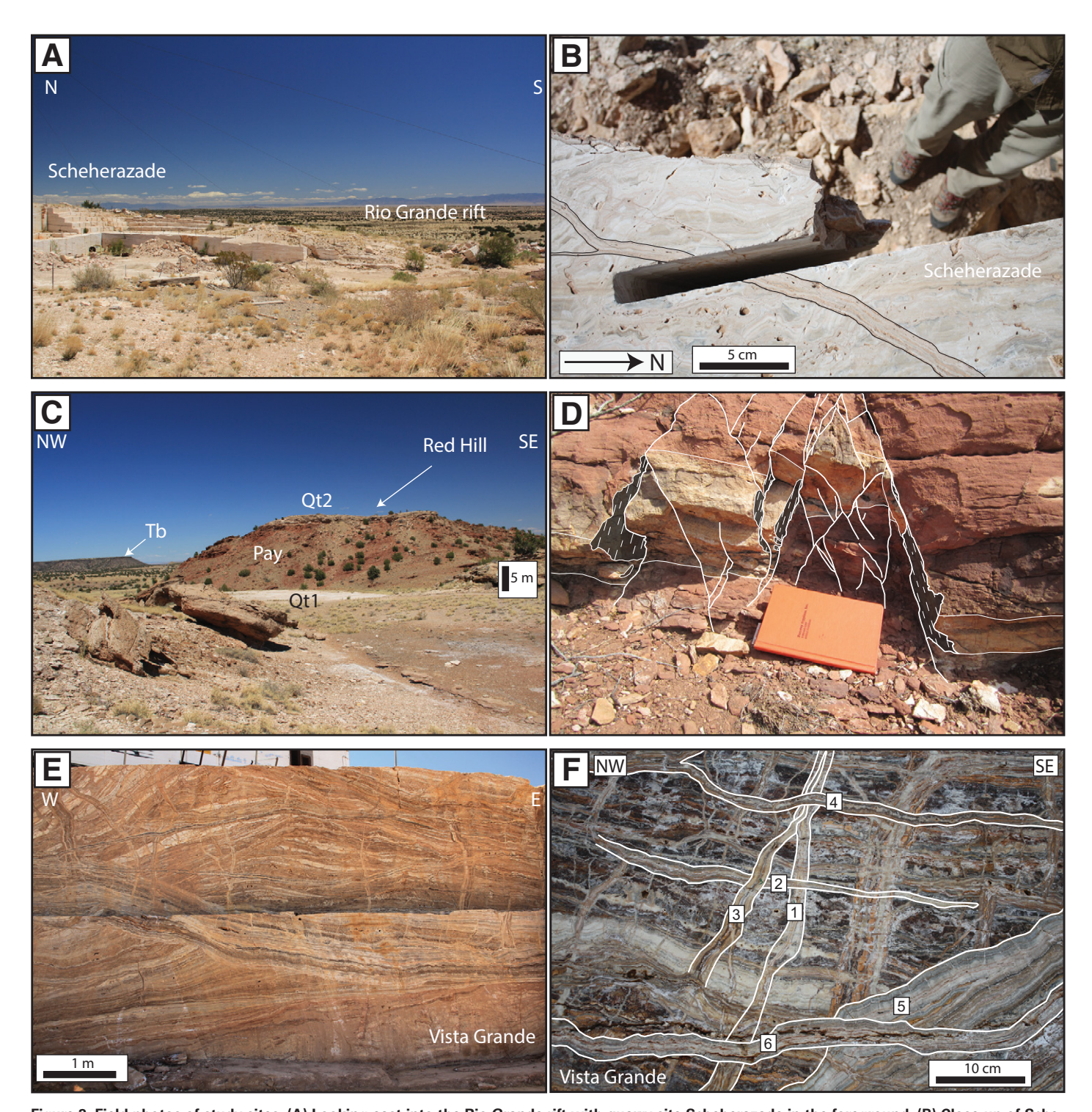


Figure 3. Field photos of study sites. (A) Looking east into the Rio Grande rift with quarry site Scheherazade in the foreground. (B) Close-up of Scheherazade. (C) Looking northeast toward Red Hill and 3.7 Ma basalt in the background. (D) Small-offset conjugate normal faults cutting Permian Yeso Formation at Red Hill. (E) View of the northern quarry wall at Vista Grande. (F) Close-up of quarry wall at Vista Grande highlighting the multiple fracture sets, which crosscut one another.

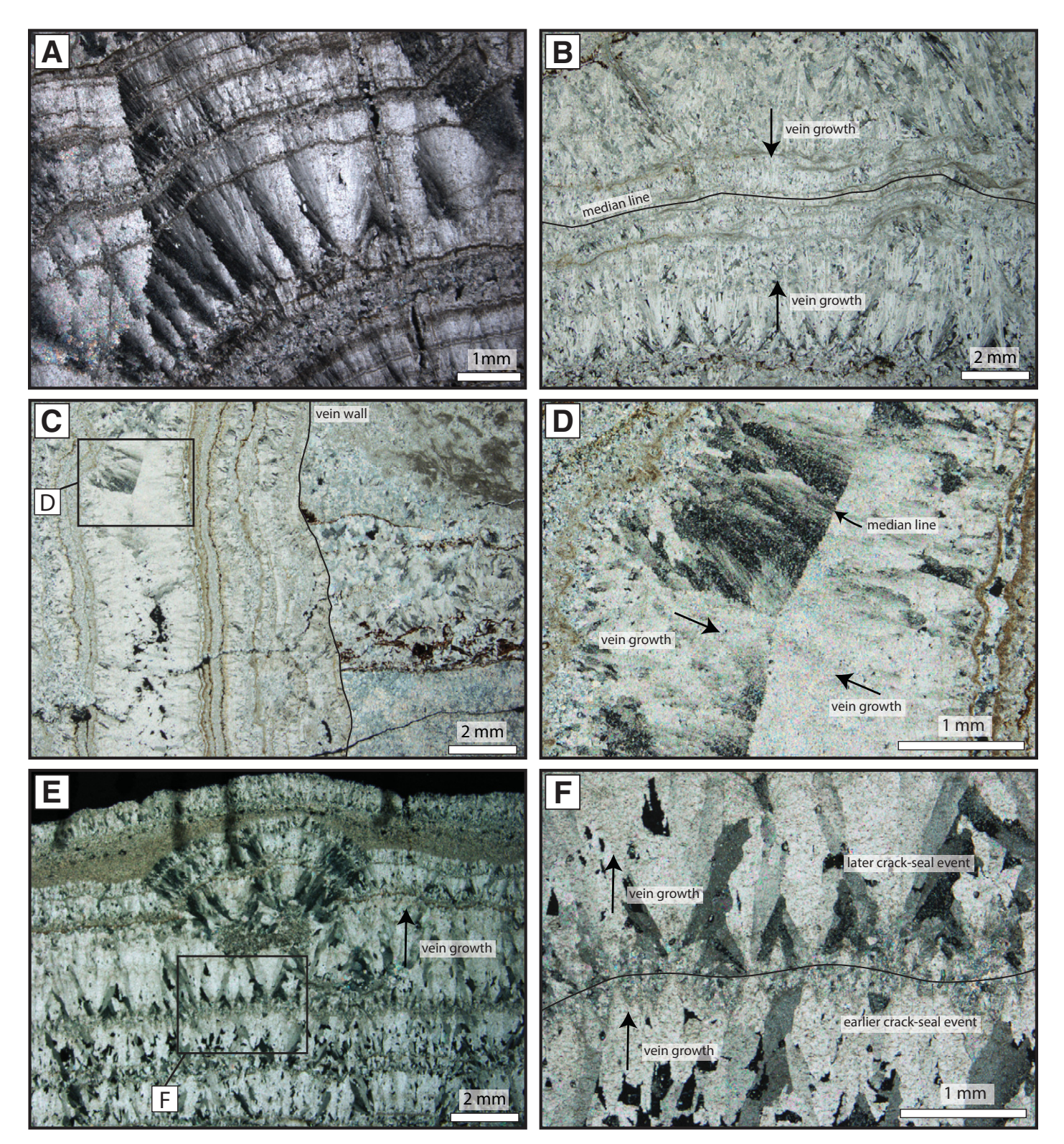


Figure 4. Photomicrographs of calcite-filled extensional veins. (A-B) Syntaxial vein growth is indicated at Vista Grande by the radiating geometry of elongate calcite fibers growing toward a central median line. (C) Perpendicular, crosscutting veins at Vista Grande. (D) Well-developed median line suggesting syntaxial vein growth. (E-F) Calcite-filled vein at Red Hill. The top of the photomicrograph is the edge of vein, and the fanning geometry of calcite fibers indicates antitaxial growth (from the center of the vein toward the vein wall). Multiple sets of radiating calcite fibers are visible, suggesting multiple episodes of fracture widening and subsequent calcite precipitation.

of extensional veins at each study site, and of normal faults at Red Hill. These directions can then be compared to the regional extension direction in the rift.

To evaluate the timing of fracturing and associated calcite precipitation within fractures, samples of fine-grained spar calcite within veins were collected from all three orthogonal extensional vein sets for dating using the uranium-thorium disequilibria method. Vein samples were collected from Temple Cream, Scheherazade, Vista Grande, and Red Hill, and material from the veins was drilled out and analyzed at the Radiogenic Isotope Laboratory at the University of New Mexico following methods described in Asmerom et al. (2010). Samples were collected from the veins because of the observation that most veins contained very little or no detrital material, which reduces the possible contamination of external ²³⁰Th.

Extensional displacements from individual veins at each of the three quarry sites were measured with the ultimate goal of calculating strain rates. At each quarry, the extensional displacements of vertical veins were measured along a horizontal line in vertical quarry faces. The initial length along this line was then estimated by subtracting the extensional displacements of all veins from the final length of the line. These values were used to calculate extension at the three quarry sites (Fig. 5), and strains were combined with the available U-series and model ages from vein infillings to calculate strain rates.

RESULTS

Extensional Veins and Faults

Here, we discuss the results of extensional veins and normal faults at each of the five study sites and inferred constraints on principal stress directions. The orientations of extensional veins and normal faults at each location are summarized on lower-hemisphere, equal-area stereographic projections (Fig. 6). Normal faults at Red Hill are plotted as planes, and each associated slickenline is plotted as an arrow that points in the movement direction of the hanging wall. Statistics computed from a Bingham axial distribution analysis from extensional veins are reported in Table 1.

Temple Cream, Scheherazade, and Vista Grande Quarry Sites

Temple Cream quarry displays three orthogonal vein sets corresponding to three orthogonal extension directions. A linked Bingham analysis combining all extensional veins suggests a dominant extension direction that is essentially E-W and horizontal (plunges 00.5° toward 090.6° ; $\lambda = 0.6778$; Table 1; Fig. 6). The quarry site Scheherazade, to the north of Temple Cream, contains three similarly oriented orthogonal vein sets. As seen in Figure 6, these veins indicate a dominant nearhorizontal extension direction that plunges 01.4° toward 100.6° (λ = 0.6576). Vista Grande quarry site contains the highest vein density of any of the study locations (Fig. 3), and it is similar to the previous two locations in that it is cut by orthogonal subvertical vein sets as well as a system of horizontal veins. Bingham analysis of these veins suggests that the dominant extension direction plunges 08.1° toward 135.9° ($\lambda =$ 0.5291; Fig. 6). At each of the three quarry sites, orthogonal vein sets crosscut one another, allowing relative ages to be determined at a given vein intersection, but crosscutting is nonsystematic, such that all three orthogonal vein sets formed contemporaneously.

Red Hill

In contrast to the three previously discussed locations, extensional veins that cut Permian Yeso Formation and overlying travertine deposit at Red Hill are relatively consistent, displaying a dominant extension direction that plunges 01.4° toward 295.6° ($\lambda = 0.8156$). Red Hill is also unique

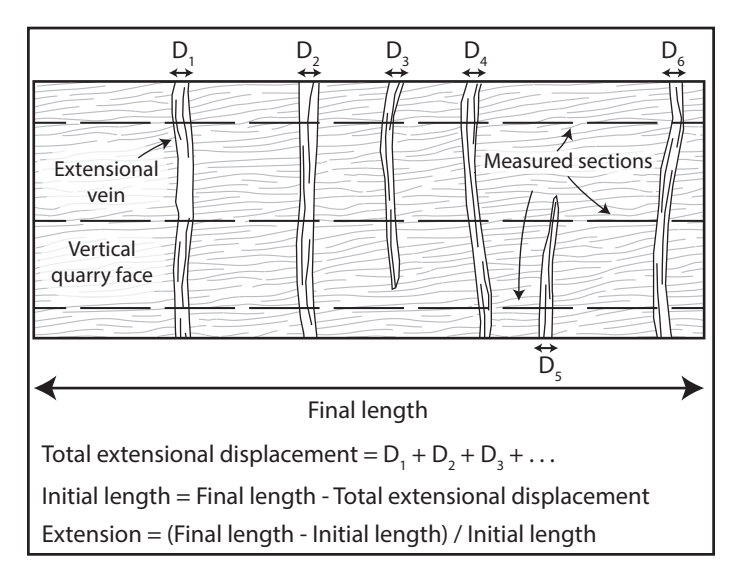


Figure 5. Schematic cross-sectional diagram illustrating the vein measurement and strain calculation process at the three quarry sites.

because it is the only location of the five dominated by small-offset normal faults rather than extensional veins. In all cases observed, normal faults are crosscut by extensional veins, indicating they formed first. Even so, the system of conjugate normal faults indicates a dominant extension direction that plunges 05.4° toward 119.9° ($\lambda = 0.3268$; Fig. 6), i.e., essentially identical to that of extensional veins, suggesting the two formed in the same stress field.

Comanche

The final location, Comanche, is similar to Red Hill in that sedimentary deposits are only cut by one system of extensional veins. The calcitefilled veins cut sedimentary beds of the Santa Fe Group that have been tilted away from horizontal (present orientation is ~020, 40°SE). This tilting is most likely due to continued movement along the Santa Fe fault, which folded the Santa Fe Group into a series of fault-parallel synclines and anticlines (Fig. 2). In most cases, veins are oriented perpendicular and parallel to bedding, and on the eastern edge of the Comanche site, the bedding returns to horizontal, and veins are vertical and horizontal, suggesting that extensional fracturing and calcite precipitation at this location occurred prior to tilting of the beds. Thus, to estimate the dominant extension direction during formation of extensional veins, sedimentary beds were restored back to horizontal. Figure 6 shows the vein measurements before and after rotation back to their inferred primary orientation, and it indicates a primary extension direction that plunges 00.4° toward 296.4° $(\lambda = 0.7662)$, similar to results obtained from Red Hill.

Uranium-Series Dating and Model Ages

U-series dating has an upper age limit of ~500,000-700,000 vr (depending on uranium content), where samples that are older than this return to a state of secular equilibrium with respect to the ²³⁸U-²³⁰Th radiogenic system and cannot be precisely or accurately dated with this method (Bourdon et al., 2003). Nevertheless, their geochemistry can be used to place important, although less precise, constraints on when they formed. For samples that are outside of this age range, U-series model ages can be calculated for samples if the ²³⁸U-²³⁴U radiogenic system is not yet in a state of secular equilibrium (within a time length of ~6-7 half-

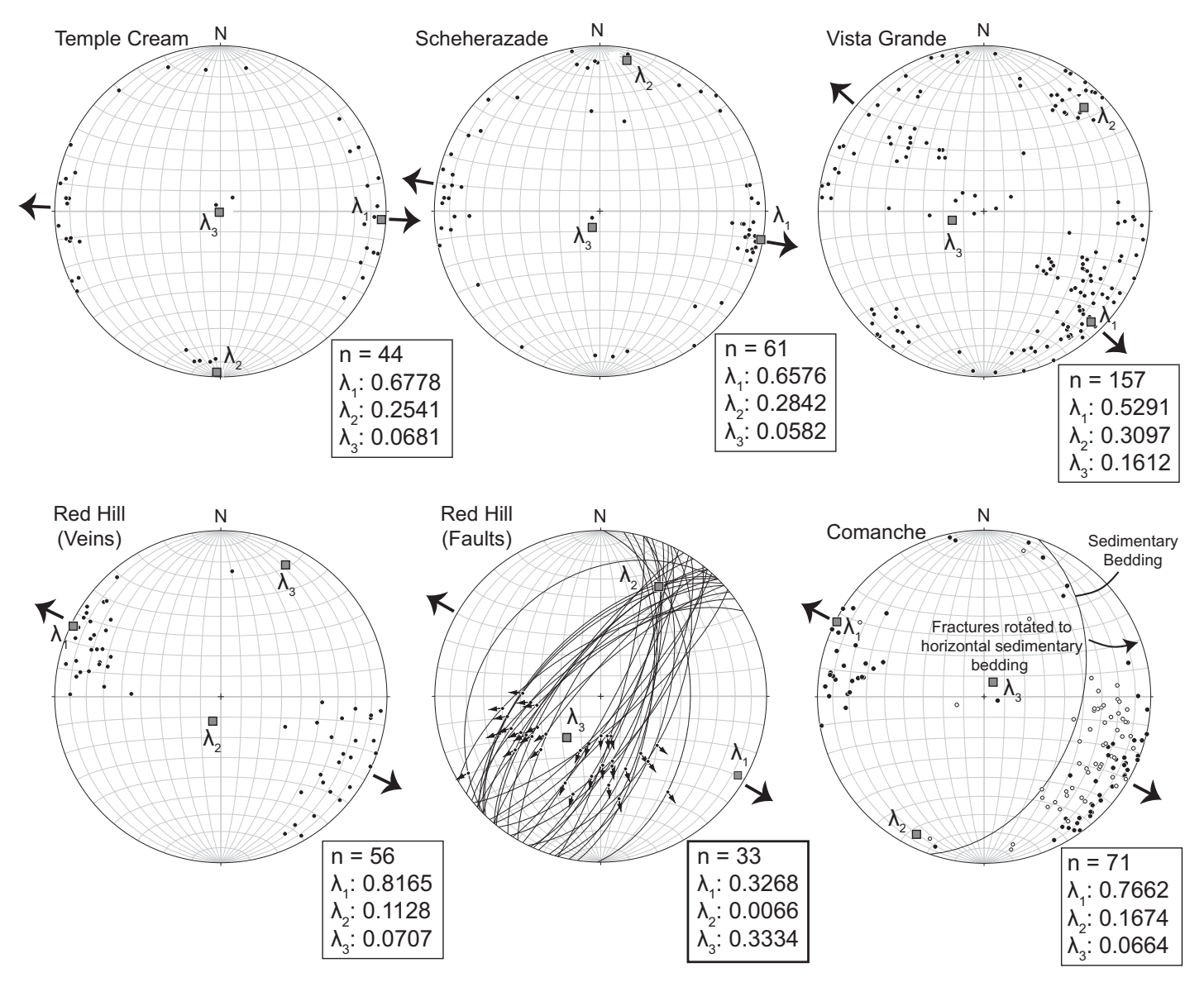


Figure 6. Lower-hemisphere, equal-area stereographic projections of extensional veins at each location and normal faults at Red Hill. Extensional veins are plotted as poles to planes. Faults at Red Hill are plotted as planes, and arrows on each fault plane are orientations of slickenlines, which indicate the direction of hanging-wall motion. The gray squares are the eigenvalue orientations calculated using a linked Bingham axial distribution. Hollow circles at Comanche are measured vein orientations before sedimentary beds were rotated back to horizontal. Plots and Bingham axial distributions are from Stereonet and FaultKin software.

lives of 234 U, or younger than ~ca. 1.5 Ma). Therefore, samples that are not yet in secular equilibrium with respect to this system cannot be older than ca. 1.5 Ma (hence 0.5–1.5 Ma), while samples that are in secular equilibrium with respect to both systems are likely older than ca. 1.5 Ma.

In total, 14 samples of calcite in extension veins were collected from the study sites for U-series dating. Four samples yielded U-series ages that range from ca. 250 ka to ca. 700 ka, six samples were outside of the $^{234}\text{U-}^{230}\text{Th}$ limit but not in secular equilibrium with respect to the $^{238}\text{U-}^{234}\text{U}$ system (indicating they are older than ~500,000 yr and younger than 1.5 Ma), and two samples were in secular equilibrium with respect to the $^{238}\text{U-}^{234}\text{U}$ system (i.e., older than ca. 1.5 Ma). Two samples (JR-BQ-1 and JR-BQ-3) had negative measured $\delta^{234}\text{U}$ values, so ages are not presented for these samples (Table 2). To further constrain the

ages of the six samples that were not in secular equilibrium with respect to the ^{238}U - ^{234}U system, U-series model ages were calculated for each of these samples. Model ages are less precise than U-series ages because the initial $\delta^{234}\text{U}$ is unknown and must be estimated. To estimate initial $\delta^{234}\text{U}$ values for samples that are outside of U-series range, we used the range of initial $\delta^{234}\text{U}$ values obtained from the four successful analyses in this study, and we combined them with successful analyses from other travertine deposits in nearby areas at Mesa del Oro and Riley South Mesa (Priewisch et al., 2012). Successful U-series analyses indicate that initial $\delta^{234}\text{U}$ values range from 41 to 849 (Table 2). We chose to disregard the 849 value due to age uncertainty, and instead used a preferred range of 41–525, or initial $\delta^{234}\text{U} = 283 \pm 242$. Model ages were calculated using the equation

$$\frac{\ln\left[\frac{(\delta^{234} U)_{m}^{-1}}{(\delta^{234} U)_{i}^{-1}}\right]}{-\lambda_{234}},$$
(1)

TABLE 1. STATISTICS COMPUTED FROM BINGHAM AXIAL DISTRIBUTION ANALYSIS

	ANALTSIS				
Ctudu cito	Number of	Eigenvalue	Orientation		
Study site	fractures	(λ)	Trend (°)	Plunge (°)	
Temple Cream (extensional veins)	44	0.6778	090.6	00.5	
		0.2541	180.6	01.7	
		0.0681	344.0	88.2	
Scheherazade (extensional veins)	61	0.6576	100.6	01.4	
		0.2842	010.4	05.9	
		0.0582	204.2	84.0	
Vista Grande (extensional veins)	157	0.5291	135.9	08.1	
		0.3097	043.9	13.9	
		0.1612	255.2	73.8	
Red Hill (extensional veins)	56	0.8165	295.6	01.4	
		0.1128	199.3	77.6	
		0.0707	025.9	12.3	
Red Hill (faults)	33	0.3268	119.9	05.4	
		0.0066	027.2	27.0	
		0.3334	220.3	62.3	
Comanche (extensional veins)	71	0.7662	296.4	00.4	
		0.1674	206.3	08.7	
		0.0664	029.3	81.3	

where $(\delta^{234}U)_m$ is the measured $\delta^{234}U$ value, $(\delta^{234}U)_i$ is the initial $\delta^{234}U$ value, and λ_{234} is the decay constant of ^{234}U , which has a value of $245,620\pm260$ yr (Cheng et al., 2013). Calculated model ages have large 2σ errors, reflecting the uncertainty in the initial $\delta^{234}U$ values used in the calculation. For some model age calculations, this wide range of initial $\delta^{234}U$ values resulted in model ages that are younger than 0.5 Ma or older than 1.5 Ma, even though the sample was in secular equilibrium with respect to the $^{238}U^{-230}$ Th system but not in secular equilibrium with respect to the $^{238}U^{-234}U$ system. These additional constraints can therefore be used to further refine the initial model age calculations, which incorporate a generous, but self-consistent, range of initial $\delta^{234}U$ values. Best-estimate model ages for six samples are provided in Table 2. Two samples were in secular equilibrium with respect to the $^{238}U^{-234}U$ system and hence are older than ca. 1.5 Ma.

Our dating results from calculated model ages and successful U-series ages range from ca. 250 ka to 1.5 Ma, and two samples are older than 1.5 Ma. All are from calcite sampled from both vertical and horizontal veins in travertine. The important conclusion of the present dating is that fracture formation in travertine mounds was episodically active for over 1.5 m.y., and hence measured strains can be considered to be representative of long-term (several-million-year time scale) strain magnitudes, directions, and rates for most or all of the Quaternary (last 2.6 m.y.).

TABLE 2. U-SERIES	GEOCHEMISTRY	AGES	AND MODEL	AGES

Sample	Location	UTM	UTM	U	Th	δ ²³⁴ U _m *	$\delta^{234}U_i^{\dagger}$	(²³⁰ Th/ ²³⁴ U)§	(²³⁰ Th/ ²³⁸ U)§	U-series	± 2σ	Calculated model	Best-fit model age
number		(E)	(N)	(ppm)	(ppm)	(± 2σ)		(± 2σ)	(± 2σ)	age (ka)		age (Ma)	constraints (Ma)
Succesful U-S	eries Ages from Qu	uarry Sites	3										
LC02-BQTC-a	Temple Cream	307975	3838028	0.53	0.02	28.2 (1.0)	58	0.9115 (0.0021)	0.9373 (0.0020)	253.6	2.7	_	_
KLC11-SH10c	Scheherazade	307776	3838674	0.5	0	114.6 (1.1)	849	1.0427 (0.0024)	1.1621 (0.0024)	709.4	193.0	-	-
KLC11-SH2b	Scheherazade	307776	3838674	0.45	0	6.3 (1.0)	41	1.0004 (0.0023)	1.0066 (0.0021)	662.7	252.1	-	-
KLC11-VG1a	Vista Grande	307765	3839305	0.550	0	42.6 (1.0)	145	1.0002 (0.0039)	1.0447 (0.0040)	434.6	14.4	-	-
Successful U-S	Series Ages From I	Nearby Lo	calities#										
AP10-MDO4a	Mesa del Oro	284164	3849773	0.54	0.01	95.2 (1.6)	195	0.9234 (0.0052)	1.0113 (0.0055)	252.8	5.3	-	-
AP10-MDO13	Mesa del Oro	284132	3849805	0.21	0.04	156.3 (0.6)	410	0.9999 (0.0039)	1.1562 (0.0044)	337.2	8.0	_	_
AP10-MDO30	Mesa del Oro	284181	3847946	0.93	0.370	78.6 (1.1)	399	1.0249 (0.0041)	1.1055 (0.0042)	565.7	68.5	_	_
AP10-	Mesa del Oro	285808	3846487	0.17	0	105.5 (2.3)	293	0.9954 (0.0049)	1.1004 (0.0049)	360.6	13.2	_	_
MDO53B-a													
	Riley South Mesa		3797562	2.68	0.03	280.1(1.1)		0.9180 (0.0080)	1.1751 (0.0102)	221.9	5.5	-	-
LC03-RS2	Riley South Mesa	310708	3797562	0.46	0.03	335.4 (0.5)	498	0.7538 (0.0029)	1.0066 (0.0039)	138.2	1.2	-	_
U-Series Mode	el Ages												
KLC11-TC2	Temple Cream	307975	3838028	0.61	0.03	0.9 (1.0)	-	1.0077 (0.0023)	1.0086 (0.0021)	_	-	>1.50**	>1.50**
KLC11-TC20a	Temple Cream	307975	3838028	0.87	0.03	2.7 (1.0)	-	1.0473 (0.0042)	1.0558 (0.0040)	-	_	1.12-2.03	1.12-1.50
JR-BQ-1	Temple Cream	307759	3838074	1.68	0	-1.6 (1.0)	-	1.0014 (0.0015)	0.9998 (0.0015)	-	_	-	-
JR-BQ-3	Temple Cream	307765	3838089	1.79	0	-2.1 (1.0)	-	1.0018 (0.0023)	0.9997 (0.0021)	-	-	-	-
JR-BQ-4	Temple Cream	307753	3838119	0.87	0.01	53.3 (1.1)	-	1.0545 (0.0016)	1.1107 (0.0013)	-	-	-0.10-0.82	0.60-0.82
JR-BQ-5	Scheherazade	307787	3838664	1.16	0.01	0.7 (1.0)	-	0.9996 (0.0023)	1.0003 (0.0020)	-	-	>1.50**	>1.50**
JR-BQ-7	Scheherazade	307776	3838664	0.69	0.01	4.5 (1.0)	-	0.9963 (0.0023)	1.0008 (0.0021)	_	-	0.86-1.77	0.86-1.50
KLC11-VG4a	Vista Grande	307765	3839305	0.88	0.010	21.4 (1.0)	-	1.0274 (0.0041)	1.0532 (0.0040)	_	-	0.24-1.15	0.60-1.15
JR-BQ-8	Vista Grande	307782	3839309	0.57	0	7.2 (1.0)	_	1.0015 (0.0023)	1.0087 (0.0021)	-	-	0.66-1.57	0.66-1.50
RedHill-1	Red Hill	307863	3840655	-	-	-	-	1.0532 (0.0044)	1.0212 (0.0042)	-	-	0.62-1.53	0.62-1.50

^{*}Measured δ^{234} U values.

[†]Initial δ^{234} U values.

[§]Values reported as activity ratios.

^{*}Nearby locality samples are from Priewisch et al. (2012).

^{**}Sample is in secular equilibrium with respect to the ²³⁴Ú-²³⁸U system.

Strain Rates

The precipitation kinetics of calcite nucleation and growth control the time and fluid required for a certain volume of calcite to grow in extensional veins (Morse and MacKenzie, 1993). These two variables are often poorly constrained because the fluids themselves are not preserved, but models that precipitate calcite in controlled laboratory environments predict that typical fluid/calcite volume ratios for the formation of thin short veins are 10⁵–10⁶ (Lee and Morse, 1999). Their model also indicates that the time necessary to precipitate calcite in nature is highly variable, ranging from thousands to perhaps millions of years for meter-scale veins. In a natural example, high-precision U-series dating of an extensional vein system in Turkey suggested that a 29-mm-thick vein formed through multiple opening events and subsequent calcite precipitation over a time period of ~12 k.y. (~2.5 mm/k.y. average rate; Uysal et al., 2011). A nearby study at Soda Dam, New Mexico, farther north along the western flank of the Rio Grande rift, shows that an ~15 cm calcite vein was developed over an ~100 k.y. time period (~0.15 mm/k.y. average rate; Tafoya, 2012). If vein formation occurred on time scales comparable to these empirical results, our veins, which are typically <5 cm thick, likely developed on time scales of tens of thousands of years, rather than millions of years. Thus, an important assumption of this study is that long-term (millionyear time scale) strain rates can be calculated incorporating measurements of multiple extensional veins across a site that each record 10-100 k.y. of strain accumulation.

Strain rates at each quarry site were calculated parallel to the dominant extension directions illustrated in Figure 6. Strain calculations were made at the three quarry sites by comparing the extensional displacement of all fractures with the total length measured (Fig. 5). We used the parameter longitudinal extension (e), where e = (final length – original length)/original length. Although it is difficult to constrain exactly when extensional fractures began to form, several authors have suggested that the travertine platforms found along the western edge of the Albuquerque Basin are Pleistocene and younger (Kelley, 1977) and that the waters moving through these fault zones have been active for the last ~2 m.y. (Callender and Zilinski, 1976). The U-series and model ages in this study are consistent with this, where the majority of extensional fractures are younger than ca. 1.5 Ma (Table 2). Therefore, to convert these extensional strain calculations to strain rates, we used a strain accumulation time of 2 m.y. to estimate maximum duration for the observed finite extensions of all veins at

the quarry sites and hence to produce estimates of Quaternary strain rates (Table 3). To compare our calculations to published data in the Rio Grande rift, all values of published extension in the literature were converted into cumulative strain rates (in units of s⁻¹) for different basins. These rates are listed in Table 4, along with the strain rates calculated in this study and current strain rates calculated across the rift and other regions using GPS.

The strain rates calculated in this study vary from $3.2 \pm 1.4 \times 10^{-16}$ s⁻¹ at Temple Cream to 6.9 \pm 3.1 \times 10^{-16} s^{-1} at Scheherazade to 3.2 \times 10^{-15} \pm $2.7 \times 10^{-16} \text{ s}^{-1}$ at Vista Grande. The 10^{-16} s^{-1} strain rates at Temple Cream and Scheherazade are comparable to the long-term strain rates reported for the central Rio Grande rift that were estimated by restored cross sections (Table 4), but the 10⁻¹⁵ s⁻¹ calculated strain rates at Vista Grande are an order of magnitude faster. The strain rates from the quarry sites are also significantly faster than the current strain rates for the Rio Grande rift of 10⁻¹⁷ s⁻¹ measured by GPS. The Basin and Range Province, which interfingers with the Rio Grande rift south of the study region, has reported current strain rates of 10⁻¹⁶ to 10⁻¹⁵ s⁻¹ that are comparable to the Quaternary rates calculated in this study (Bennett et al., 2003). Quaternary strain rates calculated in the Rio Grande rift were also compared to the GPSmeasured rates in the East African Rift. Although the driving mechanisms of extension may differ between the Rio Grande and East African Rifts, a simple comparison of strain rates is presented because these two locations are among the most well-studied and definitive examples of continental rifts worldwide. Measured GPS-constrained strain rates in the East African Rift vary by several orders of magnitude. At the slow end, 10^{-17} s⁻¹ rates are comparable to the current rates measured in the Rio Grande rift (Berglund et al., 2012), and they are slower than calculated rates in this study. The fastest extensional strain rates were measured within the central Main Ethiopian Rift, where rates are as high as 4.9×10^{-14} s⁻¹ (Kogan et al., 2012). The Afar triple junction $(6.3 \times 10^{-17} \text{ to } 6.0 \times 10^{-15} \text{ s}^{-1})$ and the southern Main Ethiopian Rift $(9.5 \times 10^{-17} \text{ to } 7.3 \times 10^{-15} \text{ s}^{-1})$ have fastest strain rates, which are comparable to the 10⁻¹⁵ s⁻¹ rates calculated at quarry site Vista Grande.

DISCUSSION

This section discusses several important implications of our calcite vein and strain rate data, beginning with the possible causes of stress that could result in the observed extensional vein and fault orientations. Next, we discuss the role of high fluid pressures on the fracture process and

TABLE 3. CALCULATED STRAIN RATES AT	OLIARRY STLIDY SITES
TABLE 3. CALCULATED STRAIN RATES AT	QUANNI SIUDI SIILS

Study site	Final length (Lf) (cm)	No. of veins measured	Total extensional displacement (cm)	Initial length (Li) (cm)	Extension	Accumulation time (m.y.)	Strain rate (s ⁻¹)	Average strain rate (st dev) (s ⁻¹)
Temple Cream								
Transect 1	876.3	18	22.0	854.3	0.026	2	4.08×10^{-16}	$3.19 \times 10^{-16} (1.43 \times 10^{-16})$
Transect 2	551.0	8	13.4	537.6	0.025	2	3.95×10^{-16}	
Transect 3	860.0	14	8.3	851.7	0.010	2	1.54×10^{-16}	
Scheherazade								
Transect 1	3086.1	58	141.0	2945.1	0.048	2	7.59×10^{-16}	$6.85 \times 10^{-16} (3.05 \times 10^{-16})$
Transect 2	2198.0	33	58.7	2139.3	0.027	2	4.35×10^{-16}	
Transect 3	2198.0	41	62.0	2136.0	0.029	2	4.60×10^{-16}	
Transect 4	833.0	20	53.4	779.6	0.068	2	1.09×10^{-15}	
Vista Grande								
Transect 1	1280.2	68	221.5	1058.7	0.209	2	3.32×10^{-15}	$3.23 \times 10^{-15} (2.71 \times 10^{-16})$
Transect 2	2808.0	115	437.9	2370.1	0.185	2	2.93×10^{-15}	
Transect 3	1500.0	126	268.2	1231.8	0.218	2	3.45×10^{-15}	

Note: Extension—(Lf - Li)/Li; strain rate—extension/second (s⁻¹)

TABLE 4. SUMMARY OF LONG-TERM AND ACTIVE STRAIN RATES IN EXTENSIONAL ENVIRONMENTS

Location	Total extension*	Time period	Strain rate (s ⁻¹) [†]	Reference
Long-term strain rates of the F	lio Grande rift			
San Luis Basin	0.08-0.12	ca. 30-27 Ma to Holocene	8.45×10^{-17} to 1.41×10^{-16}	Kluth and Schaftenaar (1994)
Espanola Basin	0.10	ca. 26 Ma to Holocene	1.22×10^{-16}	Golombek et al. (1983)
Northern Albuquerque Basin	0.17	ca. 28-21Ma to Holocene	1.92×10^{-16} to 2.57×10^{-16}	Russell and Snelson (1994)
Southern Albuquerque Basin	0.28-0.30	ca. 28-21Ma to Holocene	3.17×10^{-16} to 4.53×10^{-16}	Russell and Snelson (1994)
Current GPS§ strain rates of th	e Rio Grande rift			
San Luis Basin	_	2008–2012	$4.41 \times 10^{-17} \pm 6.34 \times 10^{-18}$	Berglund et al. (2012)
Espanola Basin	_	2008–2012	$3.90 \times 10^{-17} \pm 6.34 \times 10^{-18}$	Berglund et al. (2012)
Southern Albuquerque Basin	_	2008–2012	$3.96 \times 10^{-17} \pm 6.34 \times 10^{-18}$	Berglund et al. (2012)
Quaternary strain rates of the	western Albuquerqı	ue Basin		
Temple Cream	0.02	2 Ma to Holocene	$3.19 \times 10^{-16} \pm 1.43 \times 10^{-16}$	This study
Scheherazade	0.04	2 Ma to Holocene	$6.85 \times 10^{-16} \pm 3.05 \times 10^{-16}$	This study
Vista Grande	0.20	2 Ma to Holocene	$3.23 \times 10^{-15} \pm 2.71 \times 10^{-16}$	This study
Current GPS strain rates of the	East African Rift			
Afar triple junction	-	1992–2010	6.34×10^{-17} to 6.02×10^{-15}	Kogan et al. (2012)
Central Main Ethiopian Rift	_	1992–2010	6.34×10^{-17} to 4.85×10^{-14}	Kogan et al. (2012)
Southern Main Ethiopian Rift	_	1992–2010	9.51×10^{-17} to 7.26×10^{-15}	Kogan et al. (2012)
Current GPS strain rates of the	e Basin and Range			
Western Great Basin	_	1991–1999	$7.92 \times 10^{-16} \pm 1.58 \times 10^{-16}$ to $1.81 \times 10^{-15} \pm 2.85 \times 10^{-16}$	Bennett et al. (2003)
Northern Basin and Range	_	1991-1999	$3.17 \times 10^{-16} \pm 3.17 \times 10^{-17}$	Bennett et al. (2003)

Strain rate = extension/second (s-1)

calculated strain rates, and finally we include a discussion of the possible sources of fluid available for travertine deposition. Figure 7 is a summary diagram that helps bring these concepts together.

Origin and Nature of Stresses

Stress fields in tectonically active regions deviate from lithostatic conditions where stresses are equal in all directions and reflect an instantaneous resolution of combined gravitational and tectonic driving forces. Fluids that precipitated calcite within veins were most likely coupled with near-surface hydrologic processes and could, for example, have filled cracks formed from gravitationally induced near-surface downslope movement. If downslope movement was important, vein arrays would be expected to fan around sloping mound deposits and otherwise be perpendicular to topographic slopes. Instead, the uniformity of vein orientations at study sites with different slope aspects suggests that topography did not control vein orientation.

Rather than surface gravitational stresses controlling the orientations of extensional veins, extension directions are parallel to the regional E-W finite extension direction and GPS-recorded velocity vectors, suggesting that veins are most likely products of a local tectonic stress field. This is supported by the compiled "young" stress indicators from the World Stress Map (Heidbach et al., 2008) that indicate E-W- to NW-SE-directed extension in the rift throughout much of New Mexico (Fig. 1), including the alignment of Quaternary cinder cones at two separate locations in the central Albuquerque Basin near the study site (Kelley and Kudo, 1978; Aldrich and Laughlin, 1984). The parallelism of extension directions indicated by extensional veins and conjugate normal faults at Red Hill also supports the interpretation of a tectonic origin for the stresses. The broad sweep of extension orientations from E-W to NW-SE follows the orientation of rift-bounding structures, arguing that fault anisotropy may have resulted in small-scale stress reorientations (e.g., Faulkner et al., 2006).

We therefore consider the veins and normal faults at these study sites as records of tectonic strain accumulation at the 1-2 m.y. time scale.

Effect of Elevated Fluid Pressure

The travertines at each of the five study sites record a large flux of fluids through the upper crust at the time the fractures developed. Almost all fractures are completely filled with calcite, with very little detrital material, suggesting migration of CO₂-rich fluids that healed the fracture. Elevated fluid pressures alter the regional stress field by reducing the normal stress (Hubbert and Rubey, 1959), which amplifies the development of fractures that are favorably oriented with respect to the regional stress field. In the low-differential stress environment at each of the study sites, these high fluid pressures resulted primarily in the development of extensional veins. Thus, the anomalously high strain rates calculated at these sites, which are one to two orders of magnitude larger than the present-day strain rates, may have been facilitated by high fluid pressures at these locations in the rift during the Quaternary.

Although study sites Red Hill and Comanche only contain veins that suggest NW-SE-directed horizontal extension, quarry sites Temple Cream, Scheherazade, and Vista Grande contain three orthogonal vein patterns. Veins repeatedly offset one another to produce a mesh-like grid, indicating that all three vein sets formed contemporaneously (Fig. 3). At each location, however, the highest fracture density is approximately E-W to NW-SE (Fig. 6), parallel to the regional extension direction in the rift. To explain the orthogonal vein sets at the three quarry sites, we invoke a model where, during certain time periods, high pore fluid pressures create near-axial stress conditions with σ_1 vertical and $\sigma_2 \approx \sigma_2$. Under these conditions of very localized high pore fluid pressure, as extensional fractures develop perpendicular to σ_3 , stress is relieved in the σ_3 direction, and σ_3 and σ_{a} become subequal. During these times, extensional fractures can develop perpendicular to σ_2 and σ_3 (Caputo, 1995). Although these two

[§]GPS—global positioning system.

steeply dipping extensional vein sets crosscut bedding, the layered heterogeneity in the travertine deposit also most likely controlled vein orientation, as evidenced by the horizontal vein sets that are parallel to bedding. In this model, subequal principal stresses due to elevated pore fluid pressures combined with heterogeneities in the travertine deposit produced the interweaving pattern of veins most elegantly displayed at Vista Grande (Fig. 3).

Possible Sources of Fluid for Travertine Deposition

Spring discharge, and hence accumulation of travertine, at each of the five study sites has been shown using U-series dating to be episodic at 100 k.y. time scales in several locations in the southwestern United States: at Soda Dam, New Mexico (Tafoya, 2012); San Ysidro, New Mexico (Cron, 2011); La Madera, New Mexico (Crossey et al., 2011); Springerville, Arizona (Embid, 2009); Grand Canyon, Arizona (Szabo, 1990); and the Salt Wash graben, Utah (Kampman et al., 2012). This episodicity likely reflects both paleoclimate and paleotectonic influences, as deposition of travertine requires both ample spring discharge and CO₂ saturation. Well-recognized wet-dry periods in the U.S. Southwest (e.g., Polyak and Asmerom, 2001) likely caused fluctuations in head at spring discharge points, with higher heads resulting in larger-volume travertine deposition. Fracture age constraints provided in this study are not of high enough resolution to resolve this episodicity, but instead integrate vein growth over the 1-2 m.y. time scale and thereby average out the paleoclimate and paleotectonic oscillations.

As discussed previously, geochemical tracers of spring waters in the Albuquerque Basin of the Rio Grande rift indicate a mix between endogenic fluids and volumetrically dominant meteoric and river water (Newell et al., 2005; Williams et al., 2013). Along the western margin of the Albuquerque Basin, meteoric groundwater flows east into the basin from the Paleozoic and Mesozoic rocks within the Colorado Plateau and mixes with local arroyo discharge. Active springs within the study area contribute up to 16% of the total water in this region (Plummer et al., 2004) and contain ³He values that indicate ~7.6% mantle-derived helium (Fig. 2; Williams et al., 2013), while the He abundances measured in fluid inclusions from travertine at Scheherazade suggest these deposits were precipitated from geochemically similar fluids to the modern springs (Fig. 2). Faults within the study region, such as the Comanche fault, penetrate into the Precambrian basement rocks (Callender and Zilinski, 1976) and can potentially act as fluid pathways to the surface. Thus, these data sets suggest that in this region, the fluids available for travertine precipitation are a mixture of predominantly epigenic waters that have been mixed with volumetrically minor endogenic fluids.

The close spatial association between the study site and the underlying Socorro magma body suggests a possible connection among magmatism, fluid migration through the upper crust, travertine precipitation, and continued rift development. Although the Socorro magma body is thought to only be several hundred years old based on cooling models of a basaltic melt of its size (Fialko and Simons, 2001; Turcotte and Schubert, 2002), observed heat-flow data at the surface suggest that the modern Socorro magma body is only the most recent expression of a longer-lived magmatic system in this area (Reiter et al., 2010). Reiter et al.'s calculations indicate intrarift magmatism in this region for at least the past 1 m.y., and possibly longer, which overlaps with the timing of extensional veins in these travertine deposits. The longevity of magma emplacement within the crust beneath the study region suggests that the seismic activity recorded today may also have been active throughout the Quaternary.

We prefer a model where epigenic fluids near the surface mix with volumetrically minor endogenic fluids that are derived from magma melts

in the middle crust beneath the study area (Fig. 7). At depth, warm endogenic fluids may be aseismically transported to the surface along basement-penetrating faults, either by thermally or chemically driven buoyancy, where thermal buoyancy is governed by the geothermal gradient and chemical buoyancy is driven by differences in salinity (e.g., Schoofs et al., 1999). Alternatively, endogenic fluids may be transported to the surface by "fault valve" processes (e.g., Sibson, 1992), in which case the fluid pressures at depth fluctuate due to seismic cycles. Syntaxial growth of calcite fibers, well-developed median lines, and multiple generations of calcite fiber growth suggest that veins formed and developed episodically and widened incrementally through individual cracking events. The presence of the nearby Socorro seismic anomaly permits the possibility that fluid movement at depth may be controlled by seismic as well as aseismic processes, and that the veins and fractures in travertine deposits may record an important surface-to-mantle connection that facilitates the continued development of the Rio Grande rift.

CONCLUSIONS

Calcite-filled extension veins in travertine deposits at five study sites along the western margin of the Albuquerque Basin are inferred to record local Quaternary extension in the Rio Grande rift. U-series ages and model ages of calcite within veins range from ca. 250 ka to older than 1.5 Ma. The veins are dominantly extensional and were formed through multiple cracking events and calcite precipitation. Veins at each site indicate E-W- to NW-SE-oriented extension, which is consistent with the regional extension in the Rio Grande rift, although minor stress reorientations may be due to local stress perturbations within the Comanche-Santa Fe fault system. Three of the five study sites were subjected to high enough pore fluid pressures and were shallow enough to create near-axial stress conditions, which resulted in the development of three orthogonal vein sets during times of subequal stress magnitudes. Strain rates observed at the quarry sites range from $3.2 \pm 1.4 \times 10^{-16} \,\mathrm{s}^{-1}$ to $3.2 \times 10^{-15} \pm 2.7 \times 10^{-16} \,\mathrm{s}^{-1}$; these are higher than both the current observed rates in the rift, as well as the long-term strain rates calculated for different basins of the Rio Grande rift. Thus, although anomalously high strain rates are variable over very short spatial scales, they can persist for millions of years, and these rates instead are comparable to current strain rates within the Basin and Range Province and East African Rift. Fluids that precipitated travertine are a mixture of meteoric water and volumetrically minor endogenic fluids that ascend to the surface along basement-penetrating faults through aseismic processes and possibly seismic events.

These data and this model have important implications for understanding early stages of continental rifting. (1) Not only is the Rio Grande rift still extending based on GPS studies, but this study shows anomalously high, fluid-assisted strain rates in the Quaternary, suggesting that rift maturation is a highly dynamic process, both spatially and temporally. (2) The observed consistency of E-W extension for paleostrain and paleostress directions across different time scales (30 Ma to Holocene) points toward persistent tectonic forcings, although strain rates may be highly influenced by fluid flux through fault systems at local scales.

ACKNOWLEDGMENTS

Field studies and geologic mapping completed during this project were supported by the Educational Component of the National Cooperative Geologic Mapping Program (EDMAP) award number G11AC20152 to Karl E. Karlstrom, and New Mexico STATEMAP funding to Jason Ricketts and Karl Karlstrom. U-series dating of travertine samples was supported by National Science Foundation grant 0838575 awarded to Laura Crossey and Karl Karlstrom and was completed at the Radiogenic Isotope Laboratory at the University of New Mexico. We thank Miela Kolomaznik for laboratory assistance, and Jim Lardner, who own and operates New Mexico Travertine, Inc., for providing access to the quarry sites. Grants from the Sloan Foundation, Geological Society of America, and the New Mexico Geological Society

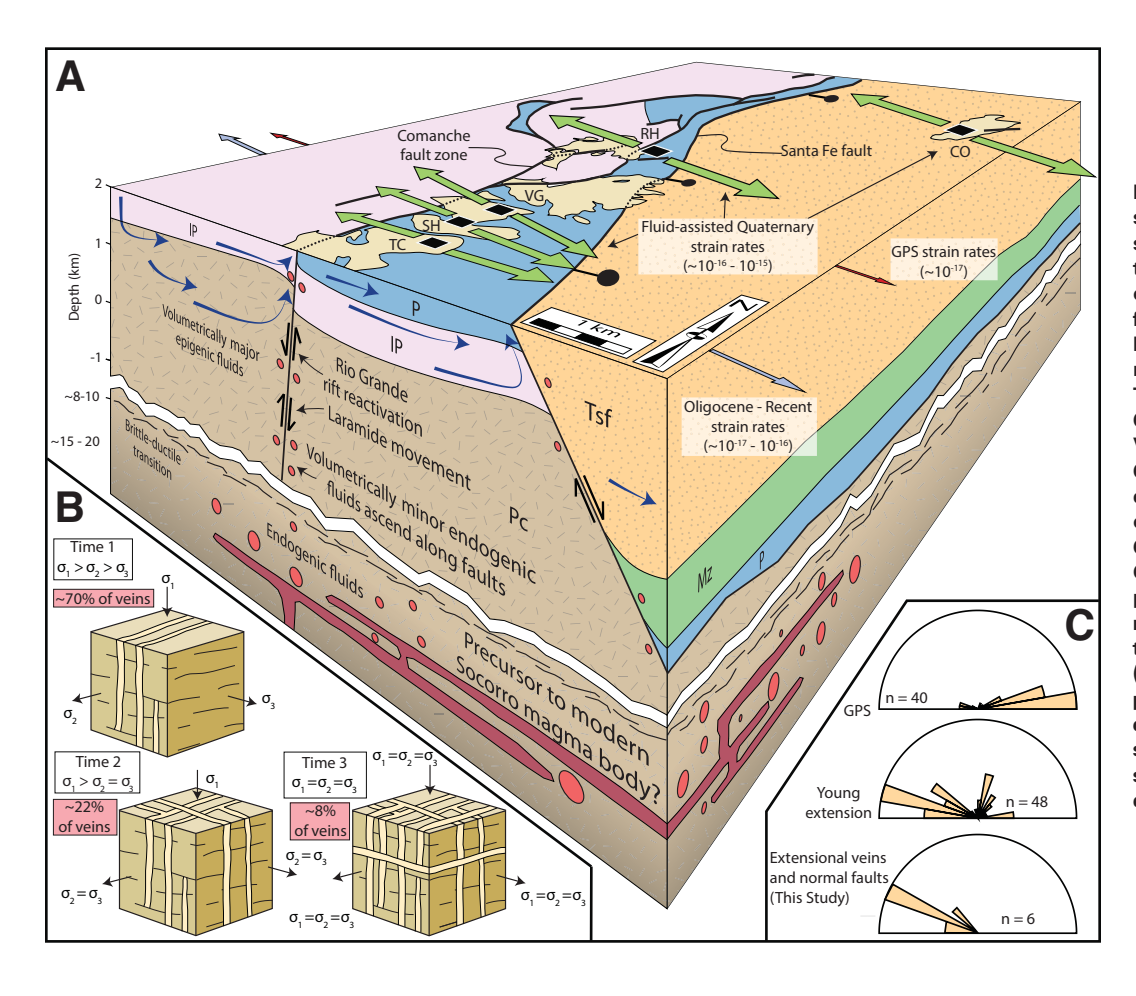


Figure 7. (A) Block diagram of the study region highlighting possible fluid sources to precipitate travertine and facilitate the development of tectonic extensional fractures at high strain rates. Pc-Precambrian; IP-Pennsylvanian; P-Permian; Mz-Mesozoic; Tsf-Santa Fe Group; TC-Temple Cream; SH-Scheherazade; VG-Vista Grande; RH—Red Hill; CO— Comanche. (B) Close-up of stress conditions required to produce orthogonal vein sets at Temple Cream, Scheherazade, and Vista Grande. Extensional veins form perpendicular to σ_3 , and orthogonal fracture sets only form during times of high pore fluid pressure. (C) Rose diagrams show subparallelism of current extension directions from global positioning system (GPS) and young extension directions (from Fig. 1), and extension directions in this study.

to Jason Ricketts are also appreciated. Constructive reviews by Christie Rowe and two anonymous reviewers led to improvements of this manuscript.

REFERENCES CITED

- Aldrich, M.J., Jr., and Laughlin, A.W., 1984, A model for the tectonic development of the southeastern Colorado Plateau boundary: Journal of Geophysical Research, v. 89, no. B12, p. 10,207–10,218, doi:10.1029/JB089iB12p10207.
- Allmendinger, R.W., Cardozo, N., and Fisher, D., 2012, Structural Geology Algorithms: Vectors and Tensors in Structural Geology: Cambridge, UK, Cambridge University Press, 302 p.
- Asmerom, Y., Polyak, V.J., and Burns, S.J., 2010, Variable winter moisture in the southwestern United States linked to rapid glacial climate shifts: Nature Geoscience, v. 3, p. 114–117, doi:10.1038/ngeo754.
- Bachman, G.O., and Mehnert, H.H., 1978, New K-Ar dates and the late Pliocene to Holocene geomorphic history of the central Rio Grande region, New Mexico: Geological Society of America Bulletin, v. 89, p. 283–292, doi:10.1130/0016-7606(1978)89<283:NKDATL>2.0 .CO;2.
- Balch, R.S., Hartse, H.E., Sanford, A.R., and Lin, K.W., 1997, A new map of the geographical extent of the Socorro mid-crustal magma body: Bulletin of the Seismological Society of America, v. 87, p. 174–182.
- Baldridge, W.S., Olsen, K.H., and Callender, J.F., 1984, Rio Grande Rift: Problems and Perspectives: New Mexico Geological Society 35th Annual Conference Guidebook, 46 p.
- Bennett, R.A., Wernicke, B.P., Niemi, N.A., Friedrich, A.M., and Davis, J.L., 2003, Contemporary strain rates in the northern Basin and Range Province from GPS data: Tectonics, v. 22, 1008. doi:10.1029/2001TC001355.
- Berglund, H.T., Sheehan, A.F., Murray, M.H., Roy, M., Lowry, A.R., Nerem, R.S., and Blume, F., 2012, Distributed deformation across the Rio Grande rift, Great Plains, and Colorado Plateau: Geology, v. 40, p. 23–26, doi:10.1130/G32418.1.
- Bourdon, B., Turner, S., Henderson, G.M., and Lundstrom, C.C., 2003, Introduction to U-series geochemistry: Reviews in Mineralogy and Geochemistry, v. 52, no. 1, p. 1–21, doi:10.2113/0520001.
- Callender, J.F., and Zilinski, R.E., 1976, Kinematics of Tertiary and Quaternary deformation along the eastern edge of the Lucero uplift, central New Mexico, *in* Woodward, L.A., and Northrop, S.A., eds., Tectonics and Mineral Resources of Southwestern North America: New Mexico Geological Society Special Publication 6, p. 53–61.
- Caputo, R., 1995, Evolution of orthogonal sets of coeval extension joints: Terra Nova, v. 7, p. 479–490, doi:10.1111/j.1365-3121.1995.tb00549.x.

- Chapin, C.E., and Cather, S.M., 1994, Tectonic setting of the axial basins of the northern and central Rio Grande rift, *in* Keller, G.R., and Cather, S.M., eds., Basins of the Rio Grande Rift: Structure, Stratigraphy, and Tectonic Setting: Geological Society of America Special Paper 291, p. 5–26, doi:10.1130/SPE291-p5.
- Cheng, H., Edwards, R.L., Shen, C.C., Polyak, V.J., Asmerom, Y., Woodhead, J., Hellstrom, J., Wang, Y., Kong, X., Spötl, C., Wang, X., and Alexander Jr., E.C., 2013, Improvements in 230Th dating, 230Th and 234U half-lives, and U-Th isotopic measurements by multicollector inductively coupled plasma mass spectrometry: Earth and Planetary Science Letters, v. 371-372, p. 82-91.
- Connell, S.D., 2004, Geology of the Albuquerque Basin and tectonic development of the Rio Grande rift in north-central New Mexico, *in* Mack, G.H., and Giles, K.A., eds., The Geology of New Mexico—A Geologic History: New Mexico Geological Society Special Publication 11, p. 359–388.
- Cron, B., 2011, Geochemical Characteristics and Microbial Diversity of CO₂-Rich Mound Springs of the Tierra Amarilla Anticline, New Mexico [M.S. thesis]: Albuquerque, New Mexico, University of New Mexico, 110 p.
- Crossey, L.J., Fischer, T.P., Patchett, P.J., Karlstrom, K.E., Hilton, D.R., Newell, D.L., Huntoon, P., Reynolds, A.C., and de Leeuw, G.A.M., 2006, Dissected hydrologic system at the Grand Canyon: Interaction between deeply derived fluids and plateau aquifer waters in modern springs and travertine: Geology, v. 34, p. 25–28, doi:10/1130/G22057.1.
- Crossey, L.J., Karlstrom, K.E., Springer, A., Newell, D., Hilton, D.R., and Fischer, T., 2009, Degassing of mantle-derived CO₂ and He from springs in the southern Colorado Plateau region—Neotectonic connections and implications for groundwater systems: Geological Society of America Bulletin, v. 121, no. 7–8, p. 1034–1053, doi:10.1130 /B26394.1.
- Crossey, L.J., Karlstrom, K.E., Newell, D.L., Kooser, A., and Tafoya, A., 2011, The La Madera travertines, Rio Ojo Caliente, northern New Mexico: Investigating the linked system of CO₂-rich springs and travertines as neotectonic and paleoclimate indicators, *in* Koning, D.J., Karlstrom, K.E., Kelley, S.A., Lueth, V.W., and Aby, S.B., eds., Geology of the Tusas Mountains and Ojo Caliente Area: New Mexico Geological Society Guidebook 62, p. 301–316.
- Embid, E.H., 2009, U-Series Dating, Geochemistry, and Geomorphic Studies of Travertines and Springs of the Springerville Area, East-Central Arizona, and Tectonic Implications [M.S. thesis]: Albuquerque, New Mexico, University of New Mexico, 116 p.
- Faulkner, D.R., Mitchell, T.M., Healy, D., and Heap, M.J., 2006, Slip on 'weak' faults by the rotation of regional stress in the fracture damage zone: Nature, v. 444, p. 922–925, doi:10.1038/nature05353.

- Fialko, Y., and Simons, M., 2001, Evidence for on-going inflation of the Socorro magma body, New Mexico, from interferometric aperture radar imaging: Geophysical Research Letters, v. 28, p. 3549-3552, doi:10.1029/2001GL013318.
- Fossen, H., 2010, Structural Geology: Cambridge, UK, Cambridge University Press, 463 p.
- Giggenbach, W.F., 1992, The composition of gases in geothermal and volcanic systems as a function of tectonic setting, in Kharaka, Y.K., and Maest, K., eds., Proceedings of the 7th International Symposium on Water-Rock Interaction: Rotterdam, Netherlands, A.A. Balkema, p. 873-878.
- Golombek, M.P., McGill, G.E., and Brown, L., 1983, Tectonic and geologic evolution of the Española Basin, Rio Grande rift: Structure, rate of extension, and relation to the state of stress in the western United States: Tectonophysics, v. 94, p. 483-507, doi:10.1016/0040 -1951(83)90031-8
- Gundimeda, M., 1995, Environmental Gas Analysis of Fluid Inclusions in Calcium Carbonates from New Mexico Including Vein Calcites from Los Alamos National Laboratory, Using Quadrupole Mass Spectrometer [M.S. thesis]: Socorro, New Mexico, New Mexico Institute of Mining and Technology, 154 p.
- Heidbach, O., Tingay, M., Barth, A., Reinecker, J., Kurfeß, D., and Müller, B., 2008, The World Stress Map Database Release 2008: http://dc-app3-14.gfz-potsdam.de/pub/download_data /download_data.html (accessed 1 February 2013), doi:10.1594/GFZ.WSM.Rel2008.
- Hubbert, M.K., and Rubey, W.W., 1959, Role of pore fluid pressure in mechanics of overthrust faulting. Part I: Geological Society of America Bulletin, v. 70, p. 115-166, doi:10.1130/0016 -7606(1959)70[115:ROFPIM]2.0.CO;2.
- Kampman, N., Burnside, N.M., Shipton, Z.K., Chapman, H.J., Nicholl, J.A., Ellam, R.M., and Bickle, M.J., 2012, Pulses of carbon dioxide emissions from intracrustal faults following climatic warming: Nature Geoscience, v. 5, p. 352-358, doi:10.1038/ngeo1451.
- Kelley, V.C., 1977, Geology of the Albuquerque Basin, New Mexico: New Mexico Bureau of Mines and Mineral Resources Memoir 33, 60 p.
- Kelley, S.A., and Chamberlin, R.C., 2012, Our growing understanding of the Rio Grande rift: New Mexico Earth Matters, v. 12, no. 2, p. 1-4.
- Kelley, V.C., and Kudo, A.M., 1978, Volcanoes and Related Basalts of the Albuquerque Basin, New Mexico: New Mexico Bureau of Mines and Mineral Resources Circular 156, 30 p.
- Kelley, S.A., Chapin, C.E., and Corrigan, J., 1992, Late Mesozoic to Cenozoic Cooling Histories of the Flanks of the Northern and Central Rio Grande Rift, Colorado and New Mexico: New Mexico Bureau of Geology and Mineral Resources Bulletin 145, 39 p.
- Kluth, C.F., and Schaftenaar, C.H., 1994, Depth and geometry of the northern Rio Grande rift in the San Luis Basin, south-central Colorado, in Keller, G.R., and Cather, S.M., eds., Basins of the Rio Grande Rift: Structure, Stratigraphy, and Tectonic Setting: Geological Society of America Special Paper 291, p. 27-38, doi:10.1130/SPE291-p27.
- Kogan, L., Fisseha, S., Bendick, R., Reilinger, R., McClusky, S., King, R., and Solomon, T., 2012. Lithospheric strength and strain localization in continental extension from observations of the East African Rift: Journal of Geophysical Research, v. 117, p. B03402, doi:10 1029/2011.JB008516
- Larsen, S., and Reilinger, R., 1983, Recent measurements of crustal deformation related to the Socorro magma body, New Mexico, in Chapin, C.E., ed., Socorro Region II: New Mexico Geological Society Thirty-Fourth Annual Conference Guidebook, p. 191-121.
- Larsen, S., Reilinger, R., and Brown, L.D., 1986, Evidence of ongoing crustal deformation related to magmatic activity near Socorro, New Mexico: Journal of Geophysical Research, v. 91, p. 6283-6292, doi:10.1029/JB091iB06p06283.
- Lee, Y., and Morse, J.W., 1999, Calcite precipitation in synthetic veins: Implications for the time and fluid necessary for vein filling: Chemical Geology, v. 156, p. 151-170, doi:10.1016 /S0009-2541(98)00183-1.
- Lewis, C.J., and Baldridge, W.S., 1994, Crustal extension in the Rio Grande rift, New Mexico: Half-grabens, accommodation zones, and shoulder uplifts in the Ladron Peak-Sierra Lucero area, in Keller, G.R., and Cather, S.M., eds., Basins of the Rio Grande Rift; Structure, Stratigraphy, and Tectonic Setting: Geological Society of America Special Paper 291, p. 135-156, doi:10.1130/SPE291-p135.
- Lozinski, R.P., and Tedford, R.H., 1991, Geology and Paleontology of the Santa Fe Group, Southwestern Albuquerque Basin, Valencia County, New Mexico: New Mexico Bureau of Mines and Mineral Resources Bulletin 132, 35 p.
- Malagnini, L., Lucente, F.P., De Gori, P., Akinci, A., and Munafo, I., 2012, Control of pore fluid pressure diffusion on fault failure mode: Insights from the 2009 L'Aquila seismic sequence: Journal of Geophysical Research, v. 117, p. B05302, doi:10.1029/2011JB008911.
- Mardia, K.V., 1972, Statistics of Directional Data: London, Academic Press, 357 p.
- Marrett, R.A., and Allmendinger, R.W., 1990, Kinematic analysis of fault-slip data: Journal of Structural Geology, v. 12, p. 973–986, doi:10.1016/0191-8141(90)90093-E.
- May, S.J., and Russell, L.R., 1994, Thickness of syn-rift Santa Fe Group in the Albuquerque Basin and its relation to structural style, in Keller, G.R., and Cather, S.M., eds., Basins of the Rio Grande Rift: Structure, Stratigraphy, and Tectonic Setting: Geological Society of America Special Paper 291, p. 113-124, doi:10.1130/SPE291-p113.
- McCalpin, J.P., 2005, Late Quaternary activity of the Pajarito fault, Rio Grande rift of northern New Mexico, USA: Tectonophysics, v. 408, p. 213-236, doi:10.1016/j.tecto.2005.05.038.
- McCalpin, J.P., Harrison, J.B.J., Berger, G.W., and Tobin, H.C., 2011, Paleoseismicity of a lowslip-rate normal fault in the Rio Grande rift, USA: The Calabacillas fault, Albuquerque, New Mexico, in Audemard, M., Michetti, F.A., and McCalpin, J.P., eds., Geologic Criteria for Evaluating Seismicity Revisited: Forty Years of Paleoseismic Investigations and the Natural Record of Past Earthquakes: Geological Society of America Special Paper 479, p. 23-46, doi:10.1130/2011.2479(01).

- Morse, J.W., and MacKenzie, F.T., 1993, Geochemical constraints on CaCO₂ transport in the subsurface: Chemical Geology, v. 105, p. 181–196, doi:10.1016/0009-2541(93)90125-3.
- Newell, D.L., Crossey, L.J., Karlstrom, K.E., and Fischer, T.P., 2005, Continental-scale links between the mantle and groundwater systems of the western United States: Evidence from travertine springs and regional He isotope data: GSA Today, v. 15, no. 12, p. 4-10, doi:10.1130/1052-5173(2005)015[4:CSLBTM]2.0.CO;2.
- Olig, S.S., Eppes, M.C., Forman, S.L., Love, D.W., and Allen, B.D., 2011, Late Quaternary earthquakes on the Hubbell Spring fault system, New Mexico, USA: Evidence for noncharacteristic ruptures of intrabasinal faults in the Rio Grande rift. in Audemard, M., Michetti, F.A., and McCalpin, J.P., eds., Geologic Criteria for Evaluating Seismicity Revisited: Forty Years of Paleoseismic Investigations and the Natural Record of Past Earthquakes: Geological Society of America Special Paper 479, p. 47-77, doi:10.1130/2011.2479(02).
- Plummer, L.N., Bexfield, L.M., Anderholm, S.K., Sanford, W.E., and Busenberg, E., 2004, Hydrochemical tracers in the middle Rio Grande Basin, USA: 1. Conceptualization of groundwater flow: Hydrogeology Journal, v. 12, p. 359-388, doi:10.1007/s10040-004 -0324-6
- Polyak, V.J., and Asmerom, Y., 2001, Late Holocene climate and cultural changes in the Southwestern United States: Science, v. 294, p. 148-151, doi:10.1126/science.1062771.
- Priewisch, A., Crossey, L.J., Embid, E., Karlstrom, K.E., Polyak, V., Asmerom, Y., Ricketts, J.W., and Nereson, A., 2012, Large-volume Quaternary travertine deposits in the Rio Grande rift and Jemez lineament, New Mexico and Arizona: Implications for paleoclimate, landscape evolution, and neotectonics: Geological Society of America Abstracts with Programs, v. 44, no. 6, p. 33.
- Ramsay, J.G., and Huber, M.I., 1983, The Techniques of Modern Structural Geology, Volume 1: Strain Analysis: London, Academic Press, 307 p.
- Reinhart, E.J., and Sanford, A.R., 1981, Upper crustal structure of the Rio Grande Rift near Socorro, New Mexico, from inversion of micro earthquake S-wave reflections: Seismological Society of America Bulletin, v. 71, p. 437-450.
- Reiter, M.R., Chamberlain, R.M., and Love, D.L., 2010, New data reflect on the thermal antiquity of the Socorro magma body locale, Rio Grande rift, New Mexico: Lithosphere, v. 2, no. 6, p. 447-453, doi:10.1130/L115.1.
- Ricketts, J.W., Karlstrom, K.E., Kelley, S.A., and Read, A.S., 2011, Cross-section restoration from Ladron Peak to the Joyita Hills and investigations of the timing and mechanism of low-angle normal faulting in the Rio Grande rift: New Mexico Geological Society Spring Meeting, Abstracts, p. 56
- Roy, M., Karlstrom, K.E., Kelley, S.A., Pazzaglia, F.J., and Cather, S.A., 1999, Topographic setting of the Rio Grande rift, New Mexico: Assessing the role of "rift-flank uplift" in the Sandia Mountains, in Pazzaglia, F.J., and Luca, S.G., eds., Albuquerque Geology: New Mexico Geological Society 50th Annual Field Conference Guidebook, p. 167-174.
- Russell, L.R., and Snelson, S., 1994. Structure and tectonics of the Albuquerque Basin segment of the Rio Grande rift: Insights from reflection seismic data, in Keller, G.R., and Cather, S.M., eds., Basins of the Rio Grande Rift: Structure, Stratigraphy, and Tectonic Setting: Geological Society of America Special Paper 291, p. 83-112, doi:10.1130/SPE291-p83.
- Sanford, A.R., Alptekin, O.S., and Toppozada, T.R., 1973, Use of reflection phases on microearthquake seismograms to map an unusual discontinuity beneath the Rio Grande rift: Bulletin of the Seismological Society of America, v. 63, p. 2021-2034.
- Schoofs, S., Spera, F.J., and Hansen, U., 1999, Chaotic thermohaline convection in lowporosity hydrothermal systems: Earth and Planetary Science Letters, v. 174, p. 213-229, doi:10.1016/S0012-821X(99)00264-2.
- Seager, W.R., Shafiqullah, M., Hawley, J.W., and Marvin, R.F., 1984, New K-Ar dates from basalts and the evolution of the southern Rio Grande rift: Geological Society of America Bulletin, v. 95, p. 87-99, doi:10.1130/0016-7606(1984)95<87:NKDFBA>2.0.CO;2.
- Sibson, R.H., 1992, Implications of fault-valve behavior for rupture nucleation and recurrence: Tectonophysics, v. 211, p. 283-293, doi:10.1016/0040-1951(92)90065-E.
- Szabo, B.J., 1990, Ages of travertine deposits in eastern Grand Canyon National Park, Arizona: Quaternary Research, v. 34, p. 24-32, doi:10.1016/0033-5894(90)90070-2.
- Tafoya, A.J., 2012, Uranium-Series Geochronology and Stable Isotope Analysis of Travertine from Soda Dam, New Mexico: A Quaternary Record of Episodic Spring Discharge and River Incision in the Jemez Mountains Hydrothermal System [M.S. thesis]: Albuquerque, New Mexico, University of New Mexico, 104 p.
- Turcotte, D.L., and Schubert, G., 2002, Geodynamics: Cambridge, UK, Cambridge University
- Uysal, I.T., Feng, Y., Zhao, J., Bolhar, R., Isik, V., Baublys, K.A., Yago, A., and Golding, S.D., 2011, Seismic cycles recorded in late Quaternary calcite veins: Geochronological, geochemical and microstructural evidence: Earth and Planetary Science Letters, v. 303, p. 84-96, doi:10.1016/j.epsl.2010.12.039.
- Williams, A.J., Crossey, L.J., Karlstrom, K.E., Newell, D., Person, M., and Woolsey, E., 2013, Hydrogeochemistry of the Middle Rio Grande aquifer system-Fluid mixing and salinization of the Rio Grande due to fault inputs: Chemical Geology, v. 351, p. 281-298, doi:10.1016/j.chemgeo.2013.05.029.

MANUSCRIPT RECEIVED 16 FEBRUARY 2013 REVISED MANUSCRIPT RECEIVED 10 OCTOBER 2013 MANUSCRIPT ACCEPTED 15 NOVEMBER 2013

Printed in the USA